The HD molecule in small and medium cages of clathrate hydrates: Quantum dynamics studied by neutron scattering measurements and computation

Daniele Colognesi,[1] Anna Powers,[2] Milva Celli,[1] Minzhong Xu,[2] Zlatko Bačić,[2,3,a)] and Lorenzo Ulivi[1,b)]

[1]*Consiglio Nazionale delle Ricerche, Istituto dei Sistemi Complessi, via Madonna del Piano 10, I-50019 Sesto Fiorentino, Italy*
[2]*Department of Chemistry, New York University, New York, New York 10003, USA*
[3]*NYU-ECNU Center for Computational Chemistry at NYU Shanghai, Shanghai 200062, China*

(Received 8 July 2014; accepted 16 September 2014; published online 1 October 2014)

We report inelastic neutron scattering (INS) measurements on molecular hydrogen deuteride (HD) trapped in binary cubic (sII) and hexagonal (sH) clathrate hydrates, performed at low temperature using two different neutron spectrometers in order to probe both energy and momentum transfer. The INS spectra of binary clathrate samples exhibit a rich structure containing sharp bands arising from both the rotational transitions and the rattling modes of the guest molecule. For the clathrates with sII structure, there is a very good agreement with the rigorous fully quantum simulations which account for the subtle effects of the anisotropy, angular and radial, of the host cage on the HD microscopic dynamics. The sH clathrate sample presents a much greater challenge, due to the uncertainties regarding the crystal structure, which is known only for similar crystals with different promoter, but nor for HD (or H_2) plus methyl *tert*-butyl ether (MTBE-d12). © *2014 AIP Publishing LLC*. [http://dx.doi.org/10.1063/1.4896623]

I. INTRODUCTION

Solid inclusion compounds formed by water and molecules of different substances are known as clathrate hydrates.[1] These solids are formed by a regularly ordered water skeleton, with H_2O molecules forming hydrogen bonds similar to those in ice, and generally assume one of the three main structures, known as cubic structure I (sI in short, space group $P\,m\bar{3}n$), cubic structure II (sII, space group $F\,d\bar{3}m$), and hexagonal structure (sH, space group $P\,6/mmm$). The *guest* molecules do not form chemical bonds with water, and are located in voids, of about 7.4 ÷ 11.0 Å diameter, referred to as *cages*, that have various geometries. In recent years, the research for efficient and environmentally friendly materials for hydrogen storage has led scientists to investigate also clathrate hydrates containing molecular hydrogen. In this respect, the quantum behavior of the light H_2 molecule confined in a clathrate cavity of nanoscale dimension has attracted a great deal of interest, and has been investigated by means of Raman spectroscopy[2,3] and inelastic neutron scattering (INS).[4,5] The latter technique, in particular, is extremely effective to study, at a microscopic level, the properties of hydrogen molecules due to the exceptionally large incoherent neutron scattering cross section of the proton. This makes INS a highly selective probe of the excitations of encapsulated hydrogen molecules, whose bands in the INS spectra dominate over those arising from the host vibrational modes not involving hydrogen. In addition, neutrons have the ability to induce spin flip in molecular nuclei, making it possible to observe in the INS spectra the $\Delta j = 1$ rotational transitions which are forbidden in infrared and Raman spectroscopy, since they involve conversion between *para*-hydrogen (p-H_2) and *ortho*-hydrogen (o-H_2).

Recently, the spectroscopic features of hydrogen clathrates measured using INS have been interpreted with the help of a quantitative theory based on the rigorous treatment of the coupled translation-rotation (TR) dynamics of the guest hydrogen molecule in a rigid cage.[6–9] This theory has demonstrated to be highly accurate when applied to *binary* (i.e., containing two guest species) cubic sII clathrate-hydrates, containing hydrogen, and tetrahydrofuran (THF). The lattice structure of this crystal is composed of *small* cages in the form of identical distorted dodecahedra (5^{12}, in an usual notation, i.e., having 12 pentagonal faces), and *large* cages in the form of polyhedra (hexakaidecahedra) having 12 pentagonal and 4 hexagonal faces ($5^{12}6^4$, in short).[10] In stoichiometric binary sII clathrates, THF molecules reside in the large cages, and the small cages host a single hydrogen molecule. Experimentally, using common preparation techniques, real clathrates comply with this condition.[11,12]

It is known that other clathrate structures can also accommodate H_2 molecules in some of their cages, and possibly serve as convenient hydrogen storage materials. In particular, this happens for clathrates having the hexagonal structure sH, which are stable with at least two kinds of guest molecules, in this case H_2 and a larger promoter molecule.[1] The sH clathrate structure has a unit cell composed of 34 H_2O molecules, which form three small 5^{12} cages, each one made of 20 water molecules and similar to those in the sII hydrates,

a)Electronic mail: zlatko.bacic@nyu.edu
b)Electronic mail: lorenzo.ulivi@isc.cnr.it

two quite asymmetric medium $4^3 5^6 6^3$ cages, also formed by 20 water molecules each, and one $5^{12}6^8$ large cage made of 36 water molecules.[1] In clathrates having the sH structure, the large promoter molecules singly occupy the $5^{12}6^8$ cages, while small gas molecules can reside in both the small and the medium cages. The single occupancy of these cages by hydrogen molecules has been demonstrated in two experimental papers via X-ray diffraction, Raman spectroscopy, and thermodynamic measurements.[13,14] Experimental INS spectra of the excitation of the H_2 molecule trapped in hexagonal clathrate-hydrate, and their comparison with the rigorous quantum theory, have been recently reported by our group.[15] While the low energy excitations in the spectrum of the sH hydrate can also be interpreted as arising from H_2 rattling and rotations in the cages, in general, the agreement with the rigorous theory for the sH structure is less satisfactory than for the sII structure. The reasons for this will be analyzed in this paper, which is devoted to the discussion of the results of experiments and theory applied to both binary sII and sH clathrate-hydrates with HD as guest. The isotopic substitution of H_2 with HD provides an additional stringent test for the theory. Moreover, our earlier theoretical studies have revealed that due to the pronounced mass anisotropy of HD, its quantum TR dynamics displays qualitatively different features from those of the homonuclear H_2 and D_2, such as strongly mixed rotational character of the TR eigenstates, in both sII hydrate[16] and the fullerene C_{60}.[17] Finally, for HD there is no distinction between *ortho* and *para* species, whose concentration, when it is not known, can act as a free parameter when comparing theory to experiment for H_2.

This paper is organized as follows: after the description of the sample preparation and the neutron instruments in Sec. II, we present and discuss the experimental results and the information that can be readily derived from these (Sec. III). In Sec. IV, we recall the theory used to compute the INS spectra and also develop analytical results on the basis of a simplified theory which assumes the separability of rotational and center-of-mass degrees of freedom of the guest molecule. Finally, Sec. V is devoted to the comparison between experiments and quantum simulations and to the discussion of their similarities and differences. Section VI summarizes the paper and draws some conclusions.

II. EXPERIMENTS

A. Sample preparation

Two different binary clathrate hydrate samples, containing HD gas, have been prepared for this experiment, namely, a sII clathrate by using perdeuterated tetrahydrofuran (TDF) as the promoter substance, and a sH clathrate where we have used methyl *tert*-butyl ether in its perdeuterated form (MTBE-d12). Samples were prepared at ISC-CNR using deuterated water, following two somewhat different procedures, respectively, for the two mentioned samples. For sII clathrate, the procedure is similar to what described in Refs. 4 and 7. In brief, a stoichiometric, simple D_2O+TDF clathrate, which has the same sII structure of the desired sample, was prepared and finely ground, at low temperature and under dry nitrogen atmosphere, and subsequently inserted into a high-pressure beryllium-copper vessel, adequate to hold hydrogen gas at pressures up to 3000 bar at any temperature between 77 and 300 K. The sample was then exposed to HD at a pressure of 800–1000 bar for 2–3 days at a temperature $T \simeq -10\,^{\circ}$C. This procedure assures the diffusion of H_2 into the crystal and the occupation of the small cages by this molecule. The preparation of sH clathrates differs from what described above in a few aspects. Hexagonal clathrate hydrates are stable only when they include two guests, so MTBE-d12 and HD must be both in contact with water during the transition to the clathrate phase. MTBE-d12 is hardly soluble in water, so we have filled the beryllium-copper vessel with a known amount of finely ground D_2O ice, and subsequently added liquid MTBE-d12, in slight abundance with respect to the stoichiometric proportions, in order to compensate for its possible evaporation, using the same precautions (low temperature and no air and moisture contamination) as in the previous case. After closing the high pressure vessel, HD gas was added at the pressure of $p \simeq 1300$ bar and the sample was kept for 2–3 days under constant pressure at a temperature $T \simeq 0\,^{\circ}$C, well outside the stability region of the simple sII HD clathrate. The sample recovery method was the same for the two samples and was accomplished by quenching the vessel in liquid nitrogen, releasing pressure, and collecting the clathrate powder to fill an aluminum slab cell. The sample cells were finally shipped to ISIS, RAL (UK) in a Dewar flask at liquid nitrogen temperature.

B. Neutron spectrometers

Measurements have been performed using TOSCA and MARI inelastic spectrometers, at ISIS, RAL (UK), respectively, for the sH D_2O+MTBE-d12+HD clathrate and for the sII D_2O+TDF+HD clathrate. TOSCA is a crystal-analyzer inverse-geometry spectrometer,[18] where the final neutron energy, E_1, is fixed. This is selected by two sets of pyrolytic graphite crystals placed in forward-scattering (at around 42.6° with respect to the incident beam) and in back-scattering (at about 137.7° with respect to the incident beam). This arrangement sets the nominal scattered neutron energy to $E_1 = 3.35$ meV (forward-scattering), and to $E_1 = 3.32$ meV (back-scattering). Higher-order Bragg reflections are filtered out by 120 mm-thick beryllium blocks wrapped in cadmium and cooled down to a temperature lower than 30 K. The incident neutron beam spans a broad incoming energy (E_0) range allowing to cover an extended energy transfer ($E = E_0 - E_1$) region: 3 meV$< E <$ 500 meV. Because of the fixed geometry of this spectrometer, only two Q values are explored (labeled Q_F and Q_B), which are not constant, but depend on the energy transfer through monotonic functions, roughly proportional to the square root of the incoming neutron energy: $Q_{F,B} \propto E_0^{1/2}$. TOSCA has an excellent energy resolution in the accessible energy transfer range ($\Delta E/E_0 \simeq 1.5\%-3\%$). The sample environment is equipped with a closed-cycle refrigerator that has been used to record spectra from our samples at a temperature lower than 20 K.

MARI is a direct-geometry spectrometer[19] also based on the time-of-flight technique: the incoming neutron energy is

selected by a Fermi chopper prior to the scattering event, while the final neutron energy is determined from the arrival's time of the neutrons which are first scattered and then detected. The angular range available on the instrument ($3.43^\circ < \theta < 134.13^\circ$) is almost continuously covered by ^{3}He-gas detectors in steps of 0.43°. Using two distinct values of the incident energy, we have been able to explore different zones of the (Q, E) kinematic plane, namely ($0.2\ \text{Å}^{-1} < Q < 6.6\ \text{Å}^{-1}$, $E < 24$ meV), and ($0.3\ \text{Å}^{-1} < Q < 8.8\ \text{Å}^{-1}$, $E < 44$ meV), for $E_0 = 25$ and 45 meV, respectively. The MARI instrumental energy resolution is determined by the type of Fermi chopper employed in the measurements. In our case the intermediate option was selected, resulting in the following values of ΔE at zero energy transfer (i.e., at the so-called *elastic line*): 1.27 and 2.28 meV for $E_0 = 25$ and 45 meV, respectively.

III. PRESENTATION AND ANALYSIS OF THE EXPERIMENTAL DATA

A. sII hydrate measured on MARI

MARI measurements were performed on one sample of D_2O+TDF+HD binary clathrate and on one sample of simple D_2O+TDF clathrate, together with two additional runs with a vanadium sample, one before and one after the actual INS experiments. At the end of any single MARI measurement, the time-of-flight data recorded by each single detector bank at an angle θ were normalized to the incoming neutron counts of the monitor, rejected in case of noisy tubes, corrected for the detector efficiency, and binned into 285 angular intervals, ranging from θ equal 3.43° to 134.13°. Fast neutron background was also evaluated and subtracted. Subsequently, the processed time-of-flight data were transformed into energy-transfer spectra, correcting for the kinematic factor $\sqrt{E_1/E_0}$. Finally, the usual vanadium spectra normalization was performed, taking also into account the Debye-Waller factor of this metal, which introduces a minute angular dependence through the angle dependence of Q. The outputs of this part of the data analysis procedure were the so-called $\Sigma(\theta, E)$ spectra, which were used for the following operations:

(i) empty-can and D_2O signal subtraction after considering sample attenuation;
(ii) sample self-shielding evaluation and correction;
(iii) multiple-scattering evaluation, simulation, and subtraction (if appropriate).

Points (i) and (ii) were implemented making use of the D_2O+TDF spectrum by assuming a homogeneous cylindrical annulus geometry for the clathrate sample. Finally, as for point (iii), after careful estimates, multiple scattering was found to be negligible in all of the present MARI measurements. At this stage, $\Sigma(\theta, E)$ spectra were transformed into constant-Q data, $S(Q, E)$, through the interpolation routines selecting a Q-step of 0.5 Å^{-1}. The spectral contributions to $S(Q, E)$ were mainly due to the scattering from the guest HD molecules inside the clathrate.

INS spectra for HD in sII clathrate have been reported in Refs. 4 and 8. Those spectra were obtained on TOSCA for two fixed scattering angles. The present measurements, performed on MARI, allow in contrast the determination of the full Q dependence of $S(Q, E)$. The energy range, however, is smaller than in the case of TOSCA and the energy resolution, even using $E_0 = 25$ meV, is lower. Typical spectra are presented in the upper panel of Fig. 1, measured for $Q = 3.0\ \text{Å}^{-1}$ using $E_0 = 45$ meV and $E_0 = 25$ meV. In the lower panel of Fig. 1, we present the fitting procedure used to derive the spectral parameters relative to the rattling and rotational bands that will be analyzed as a function of Q and compared with theory in Sec. V A. The fit, limited to the region 3–15 meV, is performed making use of the information derived from Ref. 4 where, owing to higher resolution, the position of the components of the rattling and rotational triplets have been determined with better accuracy. In particular, the differences on the energy scale between peaks have been kept fixed in the fit, and the width of all the peaks has been forced to be identical, essentially because of the limits imposed by the instrumental resolution. Nevertheless, only for the spectra measured with $E_0 = 25$ meV it has been possible to estimate the intensity of each component, while for $E_0 = 45$ meV, due to a lower resolution, while still fitting each band by a triplet, only the total intensity of each band is considered reliable.

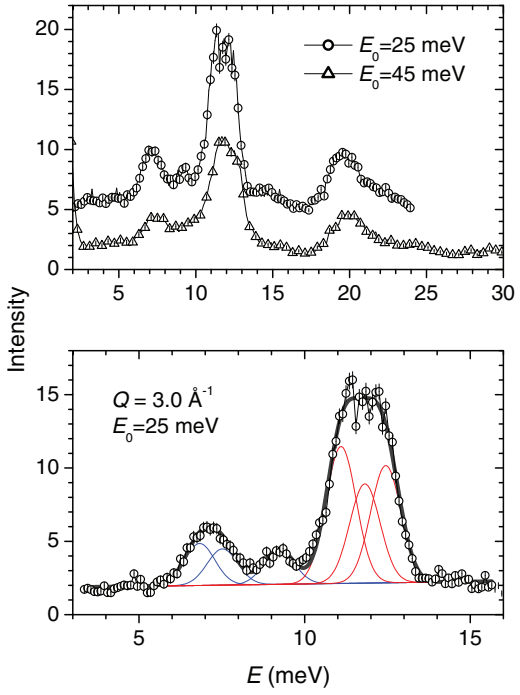

FIG. 1. (Upper panel) Typical spectra of HD molecules in a sII hydrate measured on MARI for different values of the incident energy E_0 at $Q = 3$ Å^{-1}. All the spectra have been fitted in the region 3–16 meV using Gaussians to derive the intensity of the rattling and rotations components as a function of Q. A typical best fit result is shown in the lower panel.

B. sH hydrate measured on TOSCA

Measurements on TOSCA were performed for one sample of sH D_2O+MTBE-d12+HD, at two different temperatures, namely, 20 and 80 K. The TOSCA time-of-flight spectra were transformed into energy transfer data making use of the standard data reduction routines available at the

ISIS facility. The spectra were grouped into two distinct data blocks, forward-scattering and back-scattering, respectively. This grouping procedure was justified by the narrow angular range spanned by the detectors of each block, since the corresponding full-width-at-half-maximum, $\Delta\theta$, was estimated to be only 8°. In this way, we produced the double-differential cross-section measurements along the TOSCA kinematic paths $Q = Q_{F,B}(E)$ for the two samples considered plus the empty can. Data were rebinned (i.e., interpolated), corrected for the $\sqrt{E_1/E_0}$ kinematic factor, and then the empty-can contribution was properly subtracted taking into account the E_0-dependent sample transmission as explained below. Standard corrections for self-absorption attenuation were carried out, even though both samples exhibited a quite large transmission t (e.g., $t = 87.0\%$ at $E_0 = 100$ meV for the sample containing HD) and hence a modest scattering power. This procedure was performed through the analytical approaches suggested by Sears in the case of a slab-like geometry.[20] Multiple scattering contaminations were estimated and found not important since they amounted to an average value of 5.7% of the total scattering in the 3 meV$< E_0 <$ 100 meV range. Finally, the spectral contributions coming from the D_2O host cages were removed by subtracting the spectrum of the sH Ne+D_2O+MTBE-d12 clathrate.[21] Thus, at the end of the analysis, reduced spectral data were mainly attributable to the scattering from the guest HD molecules trapped in the clathrate structure. On the basis of the structure of the sH clathrate and since the large cages are occupied by MTBE-d12, the measured spectrum can be interpreted as due to HD molecules hosted in the two different environments provided by the small 5^{12} and medium $4^3 5^6 6^3$ cages, respectively. Spectra for HD in sH clathrates have not been presented in the literature before. In the analogous case of H_2 in sH clathrates, however, the fundamental rattling and rotation bands have been identified and assigned. The experimental spectrum has been interpreted and fitted with three bands for H_2 rattling in the small cages, three different H_2 rattling bands for the medium cages and three rotation bands for both cages (small-medium cages superimposed or indistinguishable).[15] The measured HD spectrum can be interpreted exactly using the same model, by scaling the H_2 frequency of each mode making use of an empirical factor estimated in analogy to the isotopic shift observed when moving from H_2 to HD in the sII clathrate structure.[4] In that case we had observed a ratio $f \simeq 0.714$ for the rattling modes ($f = \omega(\mathrm{HD})/\omega(\mathrm{H_2})$) and $f \simeq 0.801$ for the rotational band, somewhat different from $f = 0.753$, figure expected from the Raman frequencies of the free molecule. By merely shifting the H_2 bands in this way we can identify all the peaks and bumps present in the HD spectrum from 3 to about 15 meV. The situation is reported in Fig. 2. The upper panel shows the measured INS spectra at 20 K and 80 K, while in the middle panel we report the mere superposition of the 20 K HD measured spectrum with the bands fitted for H_2 and shifted as discussed above. Only two scale factors, one for the *ortho*-H_2 rattling band and the second for the *para*-H_2 rotational band, have been used to adjust the intensity to visually match the HD experimental data. In the lower panel we report the best fit of the experimental spectrum obtained using this model. The parameters (i.e., energy position and intensity of the bands) so derived will be discussed in Sec. V B.

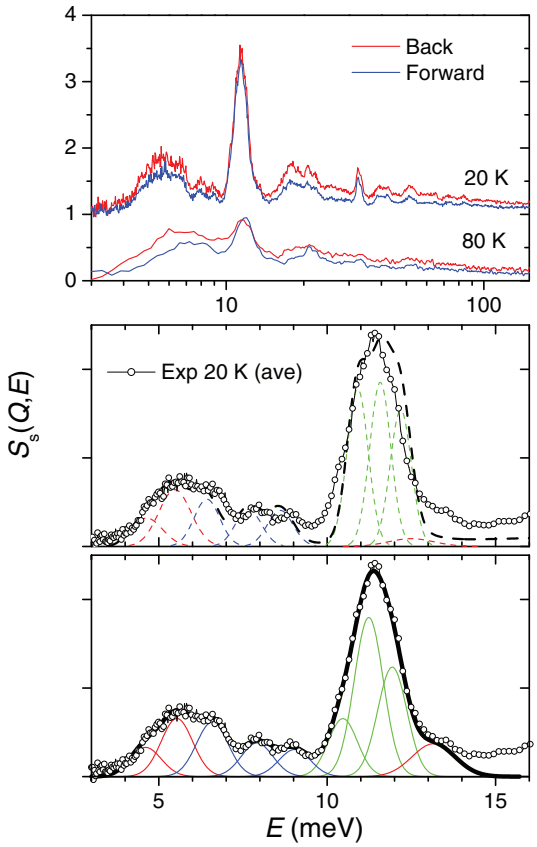

FIG. 2. In the upper panel, we show the spectra of HD in the sH clathrate measured on TOSCA, at two different temperatures, in forward- and backscattering, on a logarithmic horizontal scale. The 20 K spectrum has been shifted vertically for graphical reasons. In the middle panel, the 20 K experimental spectrum (circles) is superimposed on the bands (green for the rotation, red for the medium-cage rattling, blue for the small-cage rattling) fitted to the H_2 spectrum[15] shifted and scaled as explained in the text. The sum of these components (dashed black line) matches well the experimental points. In the lower panel, we report the result of the best fit of the HD spectrum using the same model.

IV. COMPUTATION OF THE NEUTRON SCATTERING SPECTRA AND THEORETICAL RESULTS

The treatment of the neutron scattering spectra of nanoconfined HD molecules follows closely the approach presented in Ref. 6 for H_2 molecules in nanoscale cavities, and has been already presented in detail in Ref. 8. The rigorous quantum calculation deals with one HD molecule, with fixed bond length, trapped in either one 5^{12} or $4^3 5^6 6^3$ cage, assumed to be rigid. The quantum translational-rotational (TR) dynamics of the guest molecule is treated as fully coupled. The single rigid cage approximation does not include the interaction between the host phonons and TR motions of the guest molecule, the (possibly weak) interactions between HD molecules trapped in neighboring cages, and the interaction of HD with water molecules external to the cage considered, but the very satisfactory results obtained in Refs. 7 and 8 demonstrate the applicability of this method to low-temperature clathrates, and are very promising in this sense.

The five-dimensional (5D) TR wave functions of this system have been calculated according to the procedure described in previous papers.[6,16,22]

Here we report a simplified version of this theory, developed on the basis of the well-known approximations that for H_2 and D_2 represent what is usually referred to as the *Young and Koppel* (YK) model.[23] Besides the approximations mentioned before (namely, fixed bond length and rigid cage), the only other assumption of the YK model is the free rotation of the diatomic molecule, i.e., the separability of the rotational and translational degrees of freedom. The neutron scattering spectrum is fully characterized if the double differential neutron scattering cross section of a generic heteronuclear diatomic molecule is known[24,25]

$$\left(\frac{d^2\sigma}{d\Omega dE}\right) = \frac{k_1}{k_0} S(\vec{Q}, E), \tag{1}$$

where

$$S(\vec{Q}, E) = \sum_i p_i \sum_f \left|M_f^i(\vec{Q})\right|^2 \delta(E - \epsilon_f + \epsilon_i), \tag{2}$$

and where

$$M_f^i(\vec{Q}) = \sum_{n=1}^{2} \langle f|\hat{b}_n \exp(i\vec{Q}\cdot\vec{r}_n)|i\rangle. \tag{3}$$

In Eqs. (1)–(3), $|i\rangle$ stands for the initial total (spatial plus spinorial) state of the molecular nuclei (with energy ϵ_i) and the initial spinorial state of the neutron; p_i is the statistical weight of this combined initial state; $|f\rangle$ is the final total state of the molecular nuclei (with energy ϵ_f) and the final spinorial state of the neutron; $\vec{Q} = \vec{k}_0 - \vec{k}_1$, with $\vec{k}_0$ and $\vec{k}_1$ the wave vectors of the incident and the scattered neutrons, respectively; $E = E_0 - E_1 = \hbar^2(k_0^2 - k_1^2)/(2m)$, with m the neutron mass; $\hat{b}_n$ is the scattering length operator; $\vec{r}_n$ is the position of nucleus n. By assumption, the nuclei $n = 1$ and $n = 2$ are different. For a generic nucleus n, one writes[25]

$$\hat{b}_n = b_1^{(n)} + \frac{1}{2} b_2^{(n)} \vec{\sigma}\cdot\vec{S}_n, \tag{4}$$

where $\vec{\sigma}/2$ represents the neutron spin and $\vec{S}_n$ the nuclear spin of the considered nucleus. The coefficients $b_1^{(n)}$ and $b_2^{(n)}$ in Eq. (4) are related to the coherent and incoherent scattering lengths, respectively, for the nucleus n.[25]

We consider a confined diatomic molecule HD, whose atoms D ($n = 1$) and H ($n = 2$) have the masses m_1 and m_2, respectively. Their position vectors can be written as

$$\vec{r}_n = \vec{R} + (-1)^n \left(1 - \frac{m_n}{m_1 + m_2}\right)\vec{r} \equiv \vec{R} + \eta_n \vec{r}, \quad n = 1, 2, \tag{5}$$

where $\vec{R}$ being the position vector of the center-of-mass of HD, $\vec{r}$ the vector connecting the atoms D and H, and

$$\eta_n = (-1)^n \left(1 - \frac{m_n}{m_1 + m_2}\right). \tag{6}$$

With the help of Eqs. (4) and (5), the expression for $M_f^i(\vec{Q})$ in Eq. (3) becomes

$$\begin{aligned} M_f^i(\vec{Q}) &= \sum_{n=1}^{2} \langle f|\hat{b}_n \exp(i\vec{Q}\cdot\vec{r}_n)|i\rangle \\ &= \sum_{n=1}^{2} \langle f| \left(b_1^{(n)} + \frac{1}{2} b_2^{(n)} \vec{\sigma}\cdot\vec{S}_n\right) \\ &\quad \times \exp[i\vec{Q}\cdot(\vec{R} + \eta_n\vec{r})]|i\rangle. \end{aligned} \tag{7}$$

In addition, the total wave functions of the initial ($|i\rangle$) and final states ($|f\rangle$) in Eqs. (1)–(3) can be written as the product of the neutron-spin, nuclear-spin, and spatial wave functions

$$\begin{aligned} |i\rangle &= |m_s\rangle|I_i, M_i\rangle|\Psi_i^{5D}(\vec{R}, \theta, \phi)\rangle, \\ |f\rangle &= |m_s'\rangle|I_f, M_f\rangle|\Psi_f^{5D}(\vec{R}, \theta, \phi)\rangle, \end{aligned} \tag{8}$$

where $|m_s\rangle$ and $|m_s'\rangle$ stand for the initial- and final-state neutron spin wave functions, respectively, while $|I_i, M_i\rangle$ and $|I_f, M_f\rangle$ represent the initial- and final-state nuclear spin wave functions of the HD molecule, respectively. I is the total nuclear spin of the molecule, with $I = S_1 + S_2, S_1 + S_2 - 1, \cdots, |S_1 - S_2|$. M is the projection of the total nuclear spin of the molecule on the $\hat{z}$ axis. Namely, for HD, $I = \frac{1}{2}$ or $\frac{3}{2}$. The spatial components of $|i\rangle$ and $|f\rangle$ are represented by the five-dimensional eigenfunctions $|\Psi_\tau^{5D}(\vec{R}, \theta, \phi)\rangle$ (with $\tau = i, f$) of the TR Hamiltonian for a rigid HD molecule inside a rigid nanocavity, associated with the corresponding TR energy levels ϵ_τ. The two polar angles θ and ϕ specify the direction of $\vec{r}$, i.e., the orientation of HD inside the cavity.

As we have already mentioned, an exhaustive and detailed analysis of $M_f^i(\vec{Q})$ was carried out in Ref. 8, so that here we only report its main results as far as the evaluation of the spinorial part of the matrix elements is concerned. Assuming that the incident neutrons are not polarized, we need to evaluate the new matrix element $F_{i,f}^{\mathrm{HD}}(\vec{Q})$, containing $|M_f^i(\vec{Q})|^2$ averaged over the initial neutron-spin and HD nuclear-spin states and summed over the final neutron-spin and HD nuclear-spin states

$$\begin{aligned} F_{i,f}^{\mathrm{HD}}(\vec{Q}) &= \left|\langle\Psi_f^{5D}| \exp(i\vec{Q}\cdot\vec{R})\left[b_1^{(1)} \exp(i\eta_1\vec{Q}\cdot\vec{r})\right.\right. \\ &\quad \left.\left. + b_1^{(2)} \exp(i\eta_2\vec{Q}\cdot\vec{r})\right]|\Psi_i^{5D}\rangle\right|^2 \\ &\quad + \frac{\sigma_{inc}^{(1)}}{4\pi}\left|\langle\Psi_f^{5D}| \exp(i\vec{Q}\cdot\vec{R}) \exp(i\eta_1\vec{Q}\cdot\vec{r})|\Psi_i^{5D}\rangle\right|^2 \\ &\quad + \frac{\sigma_{inc}^{(2)}}{4\pi}\left|\langle\Psi_f^{5D}| \exp(i\vec{Q}\cdot\vec{R}) \exp(i\eta_2\vec{Q}\cdot\vec{r})|\Psi_i^{5D}\rangle\right|^2, \end{aligned} \tag{9}$$

where the incoherent scattering length σ_{inc} has been introduced as[25]

$$\frac{\sigma_{inc}}{4\pi} \equiv (b_{inc})^2 = \frac{S(S+1)}{4}(b_2)^2, \tag{10}$$

This is the key equation for the calculation of the neutron scattering spectra of a heteronuclear diatomic molecule inside a nanoscale cavity. In the case of HD, $S_1 = 1$ for D and $S_2 = \frac{1}{2}$

for H, so making use of the neutron cross section tables[26] and keeping in mind Eq. (10), one obtains

$$\begin{cases} b_1^{\mathrm{H}} = -3.7406\,\mathrm{fm}; \\ b_1^{\mathrm{D}} = 6.671\,\mathrm{fm}; \\ b_{inc}(\mathrm{H}) = 25.274\,\mathrm{fm}; \\ b_{inc}(\mathrm{D}) = 4.04\,\mathrm{fm}. \end{cases} \tag{11}$$

The accurate evaluation of the five-dimensional spatial wave function $|\Psi_i^{5D}(\vec{R},\theta,\phi)\rangle$ has been described previously for the general case of the nanoconfined H_2[6] and, as far as HD is concerned, a detailed account of it can be found in Ref. 8. Here we will focus on the standard approximate YK model[23] specialized for HD. The starting point of this model is the assumption that the potential felt by a rigid diatomic molecule trapped in a likewise rigid nanocavity is independent of the polar angles θ and ϕ describing the orientation of HD relative to the cage. This statement implies two distinct facts: (a) the five-dimensional spatial wave function factorizes in the product of a center-of-mass three-dimensional wave function times an orientational (two-dimensional) wave function; (b) the latter wave function coincides with that of a free rotor, i.e., belongs to the spherical harmonics $|Y_{j,m_j}\rangle$ (in short $|j,m_j\rangle$),

$$\left|\Psi_i^{5D}(\vec{R},\theta,\phi)\right\rangle = |\psi_a(\vec{R})\rangle\left|Y_{j,m_j}(\theta,\phi)\right\rangle. \tag{12}$$

The YK approximation neglects the degeneracy removal of the rotational levels, due to the angular anisotropy of the HD-cage interaction potential, that gives rise to the experimentally observed splitting of the bands. This splitting (expressed as relative deviation from the average frequency) for the $j = 0 \rightarrow 1$ transition is about $\pm 5.2\%$ and $\pm 5.8\%$ for H_2 and HD, respectively. These figures give an idea of the accuracy of the YK model, at least when dealing with the lowest quantum levels, as for the prediction of the energy of the levels. It is possible that the accuracy is higher when comparing the total integrated intensity of the bands. Inserting Eq. (12) into Eq. (9), one can further simplify the $F_{i,f}^{\mathrm{HD}}(\vec{Q})$ calculation

$$\begin{aligned} F_{i,f}^{\mathrm{HD}}(\vec{Q}) &= F_{cm,a,b}^{\mathrm{HD}}(\vec{Q}) F_{rot,j,m_j;j',m_j'}^{\mathrm{HD}}(\vec{Q}) \\ &= |\langle\psi_b|\exp(i\vec{Q}\cdot\vec{R})|\psi_a\rangle|^2 \Big[|\langle j',m_j'|b_1^{(1)} \\ &\quad \times \exp(i\eta_1\vec{Q}\cdot\vec{r}) + b_1^{(2)}\exp(i\eta_2\vec{Q}\cdot\vec{r})|j,m_j\rangle|^2 \\ &\quad + \frac{\sigma_{inc}^{(1)}}{4\pi}|\langle j',m_j'|\exp(i\eta_1\vec{Q}\cdot\vec{r})|j,m_j\rangle|^2 \\ &\quad + \frac{\sigma_{inc}^{(2)}}{4\pi}|\langle j',m_j'|\exp(i\eta_2\vec{Q}\cdot\vec{r})|j,m_j\rangle|^2 \Big]. \end{aligned} \tag{13}$$

Making use of the well-known angular expansion of the exponential,[27] and choosing $\vec{Q}$ parallel to the $\hat{z}$ axis (which is always a legitimate choice while describing a powder averaged sample), one can write the angular matrix elements as

$$\begin{aligned} &\langle j',m_j'|\exp(i\eta_n\vec{Q}\cdot\vec{r})|j,m_j\rangle \\ &= (-1)^{m_j'}\sqrt{(2j'+1)(2j+1)}\sum_l (2l+1)\begin{pmatrix} j' & j & l \\ -m_j' & m_j & 0 \end{pmatrix} \\ &\quad \times \begin{pmatrix} j' & j & l \\ 0 & 0 & 0 \end{pmatrix} i^l j_l(\eta_n Qr), \end{aligned} \tag{14}$$

where the $3-j$ symbols and the spherical Bessel functions have been introduced. Since in the framework of the YK model, the nanocavity potential is independent of the molecular orientation, then its rotational states are degenerate with respect to m_j. So, summing over m_j' and averaging over m_j, one obtains

$$\begin{aligned} &\frac{1}{2j+1}\sum_{m_j'=-j'}^{j'}\sum_{m_j=-j}^{j}\langle j',m_j'|\exp(i\eta_1\vec{Q}\cdot\vec{r})|j,m_j\rangle\langle j,m_j| \\ &\quad \times \exp(-i\eta_2\vec{Q}\cdot\vec{r})|j',m_j'\rangle \\ &= (2j'+1)\sum_{l=|j-j'|}^{j+j'}(2l+1)\begin{pmatrix} j' & j & l \\ 0 & 0 & 0 \end{pmatrix}^2 \\ &\quad \times j_l(\eta_1 Qr) j_l(\eta_2 Qr). \end{aligned} \tag{15}$$

This result allows to finally write the rotational matrix element (now independent of the $\vec{Q}$ orientation) as

$$\begin{aligned} F_{rot,j,j'}^{\mathrm{HD}}(Q) &= (2j'+1)\sum_{l=|j-j'|}^{j+j'}(2l+1)\begin{pmatrix} j' & j & l \\ 0 & 0 & 0 \end{pmatrix}^2 \\ &\quad \times \left[\frac{\sigma_t^{(1)}}{4\pi} j_l^2(\eta_1 Qr) + \frac{\sigma_t^{(2)}}{4\pi} j_l^2(\eta_2 Qr) \right. \\ &\quad \left. + 2b_1^{(1)}b_1^{(2)} j_l(\eta_1 Qr) j_l(\eta_2 Qr)\right], \end{aligned} \tag{16}$$

where $\sigma_t^{(n)}$ represents the total scattering cross section, incoherent plus coherent, $\sigma_t^{(n)} = \sigma_{inc}^{(n)} + 4\pi(b_1^{(n)})^2$. In the low-temperature case, where only the $j = 0$ rotational level is occupied, the previous YK formula becomes even simpler

$$\begin{aligned} F_{rot,0,j'}^{\mathrm{HD}}(Q) &= (2j'+1)\left[\frac{\sigma_t^{(1)}}{4\pi} j_{j'}^2(\eta_1 Qr) + \frac{\sigma_t^{(2)}}{4\pi} j_{j'}^2(\eta_2 Qr) \right. \\ &\quad \left. + 2b_1^{(1)}b_1^{(2)} j_{j'}(\eta_1 Qr) j_{j'}(\eta_2 Qr)\right]. \end{aligned} \tag{17}$$

The last term to be discussed is the matrix element connected to the center-of-mass states, $F_{cm,a,b}^{\mathrm{HD}}(\vec{Q})$. Naturally, this quantity is strongly influenced by the details of the nanocavity potential felt by the HD molecule, which in the YK model has been approximated to be dependent only on $\vec{R}$. Even in this simplified case the computational effort to obtain $F_{cm,a,b}^{\mathrm{HD}}(\vec{Q})$ can be rather significant, since for clathrate hydrates the mentioned potential landscape does not exhibit such a high symmetry. However, for purpose of comparison, a toy model for the center-of-mass motion can be devised, assuming a spherical symmetry for the nanocavity and approximating the rattling motion of the HD molecule as essentially harmonic and

described by a single frequency, ω_0. We will refer in the following to these approximations as to the isotropic-harmonic YK model. The rattling states are now labeled by three discrete quantum numbers $\vec{n} = \{n_1, n_2, n_3\}$, all ranging from zero to infinity, numbering the number of quanta for the vibration in each direction. If the rattling vibrational frequency is the same in each direction, as we are assuming here, the energy levels are degenerate and depends only on the sum $n_1 + n_2 + n_3$. So, using the standard procedure for the neutron scattering from a harmonic oscillator,[25] one finds

$$F^{\mathrm{HD}}_{cm,\vec{n},\vec{n}'}(\vec{Q}) = \prod_{j=1}^{3} \left| \int_{-\infty}^{\infty} dR_j \frac{\alpha}{\sqrt{\pi}} \exp(iQ_jR_j) \times \exp\left(-\alpha^2 R_j^2\right) \frac{H_{n_j}(\alpha R_j)}{\sqrt{2^{n_j} n_j!}} \frac{H_{n'_j}(\alpha R_j)}{\sqrt{2^{n'_j} n'_j!}} \right|^2, \quad (18)$$

where $\alpha^2 = (m_1 + m_2)\omega_0\hbar^{-1} \equiv (m_{\mathrm{D}} + m_{\mathrm{H}})\omega_0\hbar^{-1}$.

Assuming the initial rattling state to be the ground state (which is quite reasonable at low temperatures), one can easily perform the requested Fourier transforms obtaining

$$F^{\mathrm{HD}}_{cm,\vec{0},\vec{n}'}(\vec{Q}) = \prod_{j=1}^{3} \left| \frac{(-)^{n'_j}(Q_j/\alpha)^{n'_j}}{\sqrt{2^{n'_j} n'_j!}} \exp\left(-\frac{Q_j^2}{4\alpha^2}\right) \right|^2 = \exp\left(-\frac{Q^2}{2\alpha^2}\right) \prod_{j=1}^{3} \frac{(Q_j^2/2\alpha^2)^{n'_j}}{n'_j!}. \quad (19)$$

A final, but useful, approximation, connected with the powder average, reads

$$F^{\mathrm{HD}}_{cm,\vec{0},\vec{n}'}(Q) \approx \exp\left(-\frac{Q^2}{2\alpha^2}\right) \frac{(Q^2/6\alpha^2)^{n'_1+n'_2+n'_3}}{n'_1!n'_2!n'_3!}. \quad (20)$$

V. COMPARISON BETWEEN THEORY AND EXPERIMENT

A. sII hydrate

The HD spectra have been calculated as described briefly at the beginning of Sec. IV. The structure of the sII clathrate cage, for what concerns the position of the oxygen atoms, is derived directly from the experimental structure,[10] assuming a lattice constant $a = 17.31$ Å. Water molecules are constructed with a HOH angle of 104.69° and a OH bond length 0.9716 Å oriented so to respect the Bernal and Fowler ice rules.[28] The potential energy surface has been constructed assuming the same H_2–H_2O interaction potential energy as in Ref. 16. The INS spectra have been calculated with the methodology described in Refs. 6 and 7, which was recently applied also to HD in C_{60}.[29]

To compare with the experimental results, the theoretically computed intensity of each transition between discrete TR states has been broadened by a Gaussian lineshape having a width equal to the MARI instrumental resolution, namely, 1.27 and 2.28 meV, for $E_0 = 25$ and 45 meV, respectively. The $S(Q, E)$ so derived has been grouped into a limited number of spectra, each one obtained by integration in a 0.5 Å^{-1} wide range of Q, with the average Q value ranging from 1.0 Å^{-1} to 8 Å^{-1} with 0.5 Å^{-1} steps. Beside that, an empirical intensity scale factor has to be derived. We have chosen to estimate this factor comparing the theoretical and the experimental integrated intensity of the rotational band, using for the experimental value the integrated area derived by the fitting at $Q = 2.5$ Å^{-1} (see Fig. 1). This fitting has been done allowing for the presence of a small baseline intensity in the experimental spectrum. The comparison of the spectra, for eight values of Q, is reported in Fig. 3. The agreement is quite good, at the same level of that observed for a similar HD clathrate measured on TOSCA.[8] An extra intensity is observed experimentally, at low energy, especially for large values of Q, similar to the case of H_2.[9] The origin of this extra intensity is currently under investigation by our group. To figure out a possible origin of this extra intensity, we recall that the theory does not take into account the vibrations of the water lattice. We then examine critically the procedure of the experimental data analysis. Experimentally, to isolate the contribution of the HD molecule, we have subtracted from the spectra of our sample (D_2O+TDF+HD clathrate) the spectrum of the *empty* D_2O+TDF clathrate. This procedure assumes the additivity of the contributions, which might be not completely true. Any contribution to the water lattice spectrum due to or enhanced by the presence of the HD molecules in the cages is not subtracted by our procedure of data analysis, and, not being taken into account in the theory, might appear as extra intensity in the experimental spectra.

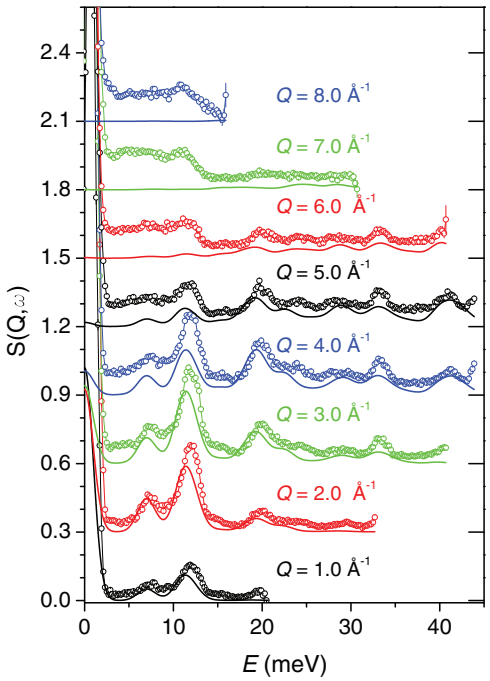

FIG. 3. Experimental spectra for HD in the small cage of the sII clathrate measured on the MARI spectrometer (empty circles with error bars) for different values of Q (the average values of Q are increasing from bottom to top and are indicated in the figure) compared with those from the rigorous quantum calculations.

In Fig. 4, we report the experimental intensity of each rotational component (black, red, and green circles) as a function of Q derived from the spectrum measured with

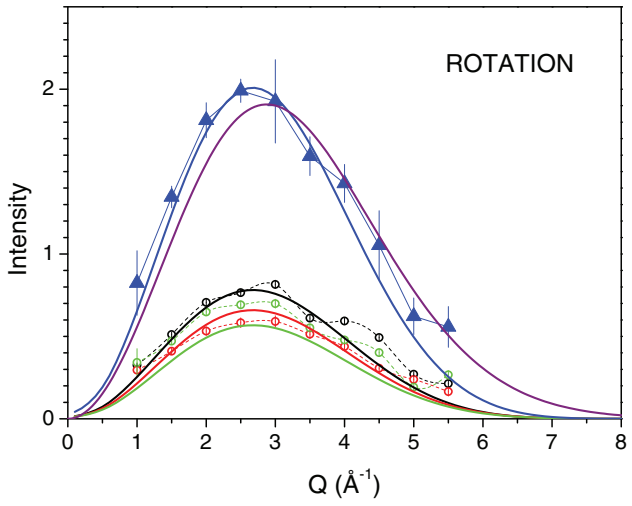

FIG. 4. Intensity of the rotational band as a function of Q. Black, red, and green circles represent the intensity of each rotational component and blue triangles is the total intensity. The solid lines of the corresponding colors are the theoretical values obtained with the rigorous calculation of the spectrum. The purple curve is the result of the approximate theory based on the isotropic-harmonic YK model, expressed by Eqs. (17) and (19), considering only the transitions starting from the ground state.

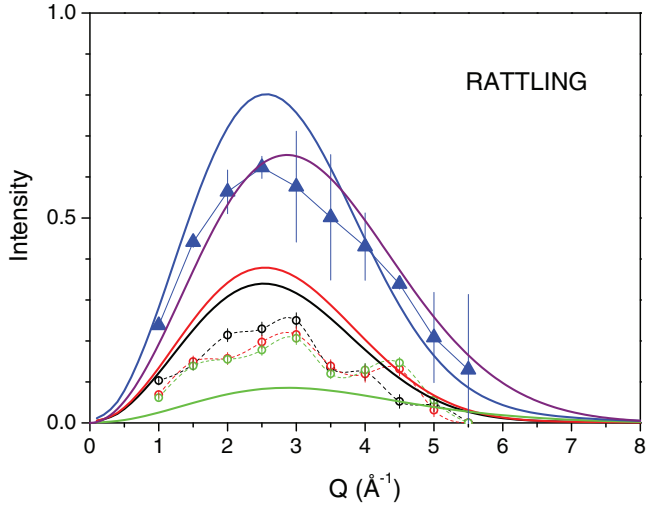

FIG. 5. Intensity of the rattling band as a function of Q. Black, red, and green circles represent the intensity of each rotational component and blue triangles are the total intensity. Solid lines of the corresponding colors are the theoretical values obtained with the rigorous spectrum computation. Purple curve is the result of the approximate theory based on the isotropic-harmonic YK model, expressed by Eqs. (17) and (19).

$E_0 = 25$ meV, due to a better resolution, and the total intensity (blue triangles), calculated as the average of the values obtained from the measurements at $E_0 = 25$ and $E_0 = 45$ meV. The solid lines of the corresponding colors are the theoretical values obtained from the rigorous calculations of the spectra. The purple curve is the result of the approximate theory based on the isotropic-harmonic YK model expressed by Eq. (17). To get the theoretical values, only the transitions originating from the ground state have been considered. This is a very good approximation at 20 K. Here theoretical and experimental results agree in the prediction that each rotational component contributes almost for 1/3 to the intensity, while they appear to disagree in predicting the exact intensity sequence among these components. The shape of the Q-dependency is very similar between theory and experiment, and is reproduced with reasonable accuracy also by the YK model in Eqs. (17) and (19). We notice however that, although the difference between the full TR coupled computation and the simplified YK model is small, it is quite larger that in the case of H_2 (see in Fig. 13 of Ref. 9). This might be due to the stronger TR coupling in the case of the caged HD relative to H_2, caused by the mass anisotropy of HD, which is not included in the simplified model. In Fig. 5, we report the experimental intensity of each rattling component as a function of Q. The derivation of this quantity and the meaning of the symbols and lines is the same as in Fig. 4. The purple curve is the result of the approximate theory based on the isotropic-harmonic YK model expressed by Eq. (19). The value of α^2, appearing in the equation, has been calculated taking for ω_0 the experimental value, i.e., 7.04 meV. In this case, for what concerns the distribution of the intensity among the three components, there is a lesser agreement than in the case of the rotational band. This might be due to the difference between the predicted and experimental energies of the components of the rattling transitions (which are 6.59, 7.28, and 8.75 meV from experiment,[4] and 6.86, 6.93, and 8.36 meV, respectively, from theory) which is larger than in the case of the rotational transition. The energy position of a transition influences the amount of state mixing and the energy transfer. Also in this case the calculated shape of the Q-dependency is very similar to the experimental one, but the total intensity of the measured rattling mode is rather smaller than the calculation. A reason for that could be the rigid cage assumption: as a matter of fact, any cage motion would tend to increase the spread of the ground state center-of-mass wavefunction and to decrease the Debye-Waller factor. Considering the isotropic-harmonic YK model, represented by the purple curve, we notice that the difference with the more rigorous theory is larger here than for the rotational band, but this curve is closer to the experimental points. This fact is possibly due to a fortuitous compensation of errors.

B. sH hydrate

In this subsection, we discuss the experimental data measured on TOSCA and compare them with the results of the quantum computation. The 5^{12} and $4^3 5^6 6^3$ cages used for the computation have been constructed on the basis of the published structures (space group *P6/mmm*) of three sH clathrates, analogous to the sample used here, but containing different guests and measured at different temperatures.[30–32] In particular, the crystallographic parameters reported by Udachin ($a = 12.212$ Å and $c = 10.143$ Å) were measured by means of X-rays diffraction at T = −100 °C for a clathrate with 2,2-dimethylpentane in the large cages, and Xe or H_2S in the small and medium ones.[30] The experiment performed by Manakov[31] deals instead with an argon clathrate, which exhibits the sH structure between 4.6 and 7.7 kbar, with the lattice constants $a = 11.976$ Å and $c = 9.870$ Å. Kirchner[32]

reports data for the adamantane-methane sH clathrate at 123 K, whose lattice constants are: $a = 12.3304$ Å and $c = 9.9206$ Å. The clathrate lattice constants depend sensitively on the molecular guest and on the temperature. The paper by Tse[33] studies two different sH clathrates, at different temperatures, and reports differences in the lattice constants of more than 1% changing either the guest or the temperature from 80 K to 250 K. That is why we have considered it appropriate to use the values of the lattice constants that we have measured in a neutron diffraction test on this very system (MTBE-d12+D_2+D_2O) at 20 K, namely, $a = 12.201$ Å and $c = 9.898$ Å, that almost coincide with those reported by Strobel[13] ($a = 12.203$ Å and $c = 9.894$ Å) measured at 90 K. The geometry of the cages depends to a lesser degree on the choice of the specific fractional coordinates.[30–32] Therefore, even without considering the difference from cage to cage that arises due to the different water proton topology, the cages are different. These differences are made visible in Fig. 4 of Ref. 15, where we have schematically reported the distribution of the distances of the oxygen atoms from the center for the small and medium cages of the sH clathrate, compared with the same quantity for the small cage of the sII clathrate. Additional information on the cage geometry is obtained considering the moments of inertia along the principal axes, whose differences show the cage asymmetry. These quantities, calculated considering only the oxygens atoms, are reported for each cage in the histogram of Fig. 6. It is evident that the $4^3 5^6 6^3$ medium cage arising for any of the three structures definitely resembles an oblate ellipsoid, while the small cage, being on the whole more symmetric, can be either prolate or oblate. The shape of the cage affects the positions of the rattling mode components, which appear as a single mode at low frequency plus a doublet at higher frequency in the case of a prolate cage, and as a doublet at low frequency plus a single mode at high frequency in the case of an oblate cage.

The spectra obtained by the quantum computations using the oxygen sublattice obtained from all the three structures are reported in Figures 7–9. The scaling of the intensity of the theoretical spectra for comparison with the experimental data was done by calculating an intensity factor so as to match the

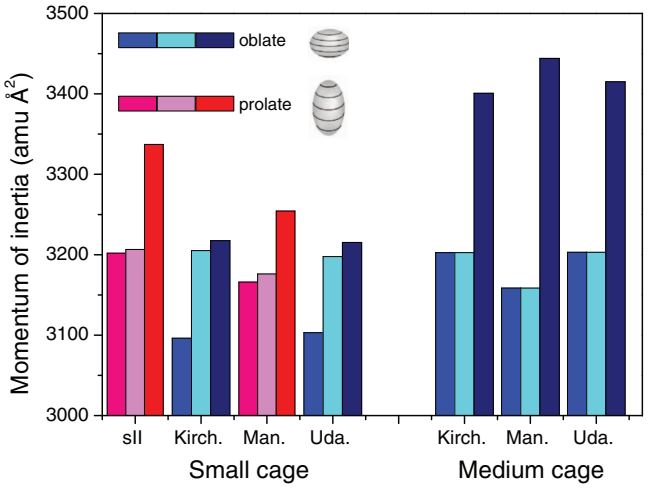

FIG. 6. Principal moments of inertia (amu × Å^2) of each cage for the three sH structures considered,[30–32] and for the small cage of the sII structure.[10]

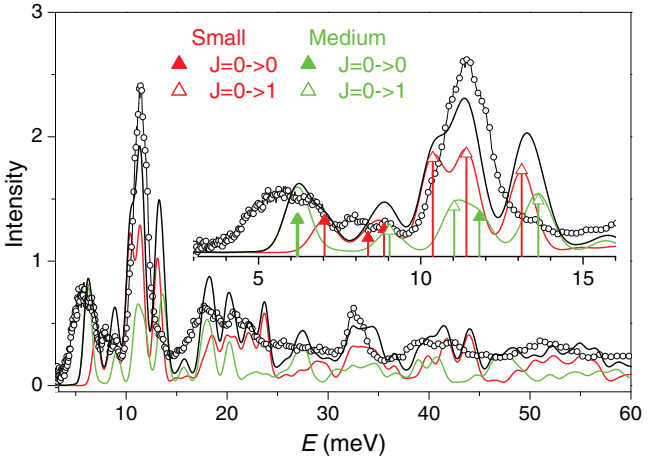

FIG. 7. Comparison of the experimental spectrum (circles) with the one calculated (solid lines) on the basis of the structure of the sH clathrate measured by Kirchner.[32] Red line represents the contribution of HD molecules in the small cage, while green line is one of the molecules in the medium cage. In the inset, triangles (empty for rotational and full for rattling transitions) show the position and the intensity of each calculated component.

integrated intensity of the fundamental rotation and rattling bands in the region 3–15 meV. The scaling constants differ slightly for the three structures considered. In these figures, circles are the experimental points, while green and red lines are, respectively, the theoretical spectra calculated for one HD molecule in the medium and small cage, scaled according to the proportion of the small and medium cages present in the structure. In the inset, we have also reported the position and the intensity of the calculated transitions, distinguishing between rattling and rotations. Only the transitions starting from the ground state are reported as sticks. The spectra in Figs. 7–9 exhibit certain common features which we discuss now. We notice that intensity at low energy is not reproduced by theory. A similar effect has been noted in the H_2 spectra (see Fig. 6 of Ref. 15) and is attributable to the poor knowledge of the actual shape of the cages, particularly of the small one. We had already observed[15] that the water proton topology influences the measured spectrum, mainly the rotational band.

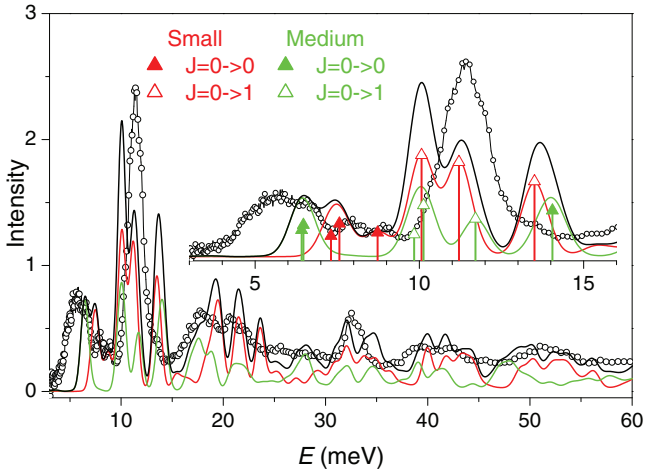

FIG. 8. Comparison of the experimental spectrum (circles) with the one calculated (solid lines) on the basis of the structure of the sH clathrate measured by Manakov.[31] The meaning of all the symbols is the same as in Fig. 7.

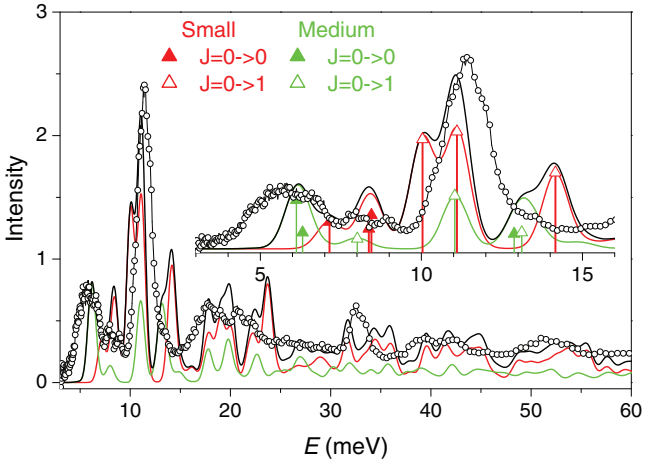

FIG. 9. Comparison of the experimental spectrum (circles) with the one calculated (solid lines) on the basis of the structure of the sH clathrate measured by Udachin.[30] The meaning of all the symbols is the same as in Figs. 7 and 8.

In this paper, we have calculated the spectra only for one specific proton configuration, since we took into account three structures. Anyhow, we find that separation of the rotational components is overestimated by the theory.

We have reported in Table I the experimental and calculated transition energies and intensities for the main excitations of HD in the small (5^{12}) and medium ($4^3 5^6 6^3$) cages. The results for all the three structures are explicitly reported. Calculated values refer to transitions from the ground state only, while experimentally a small part (3%–5 %) of the intensity, also in this frequency region, arises from transitions from thermally excited states. This is the reason why the sum of the calculated intensity is slightly smaller than the corresponding sum for the experimental intensity. Concerning the intensity, we notice from the table that the theory generally underestimates the rattling transitions and overestimates the rotational transitions.

VI. SUMMARY AND CONCLUSIONS

This paper has been devoted to the study of the dynamics of a quantum molecule confined in nanometric cages. Unlike the homonuclear isotopologue H_2, HD does not have the *ortho* and *para* nuclear spin isomers, whose relative concentration is variable and depends on the thermal history of the sample. As a result, the population of the rotational levels of HD, which affects the intensities of the bands measured in the neutron spectrum, can be related directly to the temperature of the sample. This makes the comparison between the measured and computed INS spectra more straightforward and conclusive. At the same time, the neutron spectrum is still quite intense, due to the presence of the proton in HD. The theory for the calculation of the spectrum, both on the basis of the rigorous 5D translation-rotation theory, and of the Young and Koppel model, has been worked out, respectively, in a recent paper of ours[8] and in the present paper. Therefore,

TABLE I. Energies and intensities of the fundamental bands relative to the rattling and rotational transitions. Roman numerals indicate the different components of each band. In the lines labeled "all" we have reported the weighted mean of the transition energies and the sum of the intensities.

				Theory					
		Experiment		Udachin		Kirchner		Manakov	
Cage	Comp.	Energy (meV)	Int.	Energy (meV)	Int.	Energy (meV)	Int.	Energy (meV)	Int.
				Rattling transitions					
5^{12}	I	6.59	0.72	7.15	0.34	7.03	0.40	7.31	0.26
	II	7.92	0.45	8.37	0.25	8.37	0.18	7.57	0.41
	III	9.04	0.36	8.45	0.43	8.87	0.29	8.73	0.30
	all	7.55	1.53	8.00	1.02	7.93	0.87	7.86	0.96
$4^3 5^6 6^3$	I	4.61	0.39	6.12	0.61	6.18	0.41	6.42	0.33
	II	5.54	0.77	6.31	0.21	6.22	0.41	6.47	0.39
	III	13.16	0.59	12.88	0.19	11.81	0.44	14.05	0.57
	All	7.91	1.75	7.43	1.01	8.17	1.26	9.80	1.29
				Rotational transitions					
5^{12}	I			10.04	1.38	10.37	1.18	10.07	1.25
	II			11.10	1.48	11.41	1.24	11.20	1.17
	III			14.16	0.96	13.11	1.03	13.50	0.93
	All			11.49	3.81	11.56	3.44	11.42	3.35
$4^3 5^6 6^3$	I			8.01	0.13	9.04	0.27	9.84	0.28
	II			11.04	0.67	11.03	0.57	10.13	0.64
	III			13.11	0.21	13.62	0.65	11.71	0.47
	All			11.08	1.00	11.79	1.49	10.61	1.38
Both	I	10.46	0.71						
	II	11.23	1.95						
	III	11.93	1.34						
	All	11.33	4.00	11.40	4.82	11.63	4.94	11.18	4.74

although INS results had been already presented for both sII and sH clathrates containing H_2, the extension to HD is considered a more stringent test for the theory, because of the strong mass anisotropy of HD and for the fewer assumptions needed for the data analysis (i.e., the ortho-para ratio). Our results demonstrate the limitations on the degree of agreement between the measured and calculated INS spectra stemming primarily from the uncertainties regarding the actual structure of the host crystal. As a matter of fact, for the sII D_2O+TDF+HD sample, whose structure is reported accurately in a few papers,[10,34] the calculated spectrum agrees very well with the experimental one. On the contrary, for the comparison of the spectra obtained from the sH D_2O+MTBE-d12+HD clathrate, we have been forced to use for the computation the cages constructed on the basis of the structural parameters of similar, but not identical, clathrates,[30–32] as described in Sec. V B. Even if the structural differences are small, they are clearly reflected in the computed INS spectra, and lead to discrepancies with the sensitive neutron spectroscopy.

Correlated with the question of the oxygen lattice structure there are the issues of the accuracy of the H_2–H_2O interaction potential and the water proton configuration. The interaction potential could surely be refined, especially in its anisotropic part, which is modeled by the points charges on the H_2 molecule. The model probably tends to overestimate the anisotropic interaction, even if the point charges reproduce the isolated molecule electric quadrupole. The question whether the H_2 quadrupole is decreased when the molecule is in the condensed phase has been often advanced in the literature, but is still unanswered. A very important aspect is the relevance of the water proton disorder and its configuration. We have presented here results for only one proton configuration, chosen at random among all the ones respecting the Bernal and Fowler rules. An average among several of them might be more appropriate, but, besides the limits imposed by the computation time, this approach assumes that all configurations respecting the Bernal and Fowler rules are equally probable. Finally, the clathrate water molecules beyond the single small or medium cages considered in the calculations surely contribute to the host interaction with HD (and H_2) and the INS spectra. We are currently investigating this open issue, which adds further to the complexity of the problem.

The quantitative comparison of theoretical and experimental energies and intensities performed in this work shows that there is still considerable room for improvement. This will allow us to investigate in the future the fine details of the intermolecular potential energy surface for the H_2-clathrate interaction and to improve it systematically. This will undoubtedly find applications in different areas.

ACKNOWLEDGMENTS

Z.B. is grateful to the NSF for the partial support of this research through Grant No. CHE-1112292. In addition, the work of Z.B. was supported in part at the Weizmann Institute of Science by the Joseph Meyerhoff Visiting Professorship.

[1] E. D. Sloan and C. A. Koh, *Clathrate Hydrates of Natural Gases*, 3rd ed. (Taylor & Francis, New York, 2008).
[2] A. Giannasi, M. Celli, L. Ulivi, and M. Zoppi, J. Chem. Phys. **129**, 084705 (2008).
[3] A. Giannasi, M. Celli, M. Zoppi, M. Moraldi, and L. Ulivi, J. Chem. Phys. **135**, 054506 (2011).
[4] L. Ulivi, M. Celli, A. Giannasi, M. Zoppi, D. J. Bull, and A. J. Ramirez-Cuesta, Phys. Rev. B **76**, 161401(R) (2007).
[5] L. Ulivi, M. Celli, A. Giannasi, A. J. Ramirez-Cuesta, and M. Zoppi, J. Phys.: Condens. Matter **20**, 104242 (2008).
[6] M. Xu and Z. Bačić, Phys. Rev. B **84**, 195445 (2011).
[7] M. Xu, L. Ulivi, M. Celli, D. Colognesi, and Z. Bačić, Phys. Rev. B **83**, 241403(R) (2011).
[8] M. Xu, L. Ulivi, M. Celli, D. Colognesi, and Z. Bačić, Chem. Phys. Lett. **563**, 1 (2013).
[9] D. Colognesi, M. Celli, L. Ulivi, M. Xu, and Z. Bačić, J. Phys. Chem. A **117**, 7314 (2013).
[10] T. C. W. Mak and R. K. McMullan, J. Chem. Phys. **42**, 2732 (1965).
[11] K. C. Hester, T. H. Strobel, E. D. Sloan, C. Koh, A. Huq, and A. J. Schultz, J. Phys. Chem. B **110**, 14024 (2006).
[12] T. H. Strobel, C. J. Taylor, K. C. Hester, S. F. Dec, C. Koh, K. T. Miller, and E. D. Sloan, J. Phys. Chem. B **110**, 17121 (2006).
[13] T. Strobel, C. A. Koh, and E. D. Sloan, J. Phys. Chem. B **112**, 1885 (2008).
[14] A. R. Duarte, A. Shariati, L. J. Rovetto, and C. J. Peters, J. Phys. Chem. B **112**, 1888 (2008).
[15] M. Celli, A. Powers, D. Colognesi, M. Xu, Z. Bačić, and L. Ulivi, J. Chem. Phys. **139**, 164507 (2013).
[16] M. Xu, F. Sebastianelli, and Z. Bačić, J. Chem. Phys. **128**, 244715 (2008).
[17] M. Xu, F. Sebastianelli, Z. Bačić, R. Lawler, and N. J. Turro, J. Chem. Phys. **129**, 064313 (2008).
[18] D. Colognesi, M. Celli, F. Cilloco, R. J. Newport, S. F. Parker, V. Rossi-Albertini, F. Sacchetti, J. Tomkinson, and M. Zoppi, Appl. Phys. A **74**, S64 (2002).
[19] K. H. Andersen, Nucl. Instrum. Meth. Phys. Res. A **371**, 472 (1996).
[20] V. F. Sears, Adv. Phys. **24**, 1 (1975).
[21] M. Celli, D. Colognesi, L. Ulivi, M. Zoppi, and A. J. Ramirez-Cuesta, J. Phys.: Conf. Ser. **340**, 012051 (2012).
[22] M. Xu, Y. S. Elmatad, F. Sebastianelli, J. W. Moskowitz, and Z. Bačić, J. Phys. Chem. B **110**, 24806 (2006).
[23] J. A. Young and J. U. Koppel, Phys. Rev. **135**, A603 (1964).
[24] H. Stein, H. Stiller, and R. Stockmeyer, J. Chem. Phys. **57**, 1726 (1972).
[25] S. W. Lovesey, *Theory of Neutron Scattering from Condensed Matter* (Oxford University Press, Oxford, 1984), Vol. I.
[26] V. F. Sears, Neut. News **3**, 26 (1992).
[27] G. Arfken, *Mathematical Methods for Physicists* (Academic Press, Orlando, FL, 1985).
[28] J. D. Bernal and R. H. Fowler, J. Chem. Phys. **1**, 515 (1933).
[29] M. Xu, S. Ye, R. Lowler, N. J. Turro, and Z. Bačić, Philos. Trans. R. Soc. A **371**, 20110630 (2013).
[30] K. A. Udachin, C. I. Ratcliffe, G. D. Enright, and J. A. Ripmeester, Supramol. Chem. **8**, 173 (1997).
[31] A. Yu. Manakov, V. I. Voronin, A. V. Kurnosov, A. E. Teplykh, V. Yu. Komarov, and Yu. A. Dyadin, J. Incl. Phenom. Macro. **48**, 11 (2004).
[32] M. T. Kirchner, R. Boese, W. E. Billups, and L. R. Norman, J. Am. Chem. Soc. **126**, 9407 (2004).
[33] J. S. Tse, J. Inclus. Phenom. Mol. **8**, 25 (1990).
[34] C. Y. Jones, S. L. Marshall, B. C. Chakoumakos, C. J. Rawn, and Y. Ishii, J. Phys. Chem. B **107**, 6026 (2003).